Desalination and Water Treatment
www.deswater.com

doi: 10.5004/dwt.2020.26178

202 (2020) 232–240
October

Flower-shaped nanoscale $Na_2Mg(CO_3)_2$: a promising adsorbent for fluoride removal from drinking water

Bai Sun[a,b,*], Fangwen Xu[a], Fei Liu[a], Yunming Cheng[a], Jie Zhang[a], Zhuo Tang[a], Jinyun Liu[c], Shuguang Zhu[a], Xinli Cai[a,*]

[a]*Key Laboratory of Water Pollution Control and Wastewater Resource of Anhui Province, College of Environment and Energy Engineering, Anhui Jianzhu University, Hefei 230601, China, Tel. +86-551-63828252; Fax: +86-551-63828252; emails: bsun@mail.ustc.edu.cn (B. Sun), ahcxl@163.com (X. Cai), 2392276291@qq.com (F. Xu), 765846857@qq.com (F. Liu), 502283466@qq.com (Y. Cheng), 1045441563@qq.com (J. Zhang), 1341451826@qq.com (Z. Tang), zhushuguang@ahjzu.edu.cn (S. Zhu)*
[b]*Nano-Materials and Environmental Detection Laboratory, Hefei Institute of Physical Science, Chinese Academy of Sciences, Hefei 230031, China*
[c]*Key Laboratory of Functional Molecular Solids, Ministry of Education, College of Chemistry and Materials Science, Anhui Normal University, Wuhu 241002, China, email: jyliu@ahnu.edu.cn (J. Liu)*

Received 23 January 2020; Accepted 27 May 2020

ABSTRACT

In this paper, flower-shaped $Na_2Mg(CO_3)_2$ nanoparticles were synthesized by a simple hydrothermal method for defluoridation in water. The effects of the initial concentration of fluoride, pH value, and coexisting ions on the removal of fluoride were investigated. $Na_2Mg(CO_3)_2$ nanoparticles were characterized by using scanning electron microscopy, X-ray diffraction, Fourier transform infrared spectroscopy, and energy disperse analysis of X-rays. The experimental results show that the adsorption isotherm is consistent with the Freundlich model at pH = 7 and 35°C. When the initial concentration is 200 mg/L, the maximum adsorption capacity calculated by the Langmuir model is up to 113.64 mg/g. The adsorption kinetics is consistent with the pseudo-second-order model, and the adsorption equilibrium can be achieved within 100 min. There is little effect on $Na_2Mg(CO_3)_2$ nanoparticles in the wide range of pH values (3–10). The fluoride removal rate reaches up to 92.26% at pH = 7 for the initial fluoride concentration of 5 mg/L, along with the adsorbent dose of 1 g/L. Except for PO_4^{3-}, SO_4^{2-}, and HCO^{3-}, other anions don't affect the fluoride adsorption. The experiment results also demonstrate that the prepared adsorbents can be reused for at least six times. Finally, the mechanism for fluoride adsorption by $Na_2Mg(CO_3)_2$ nanoparticles is discussed.

Keywords: $Na_2Mg(CO_3)_2$; Adsorption; Defluoridation

1. Introduction

Fluoride is one of the essential trace elements in the human body. Fluoride contamination of groundwater through a combination of natural processes and anthropogenic activities is a major problem worldwide [1,2]. According to the previous report [3], about 90% of fluoride in drinking water is absorbed in the digestive system, while only 30%–60% of fluoride in the food is absorbed in the digestive system. Proper intake of fluoride will promote normal bone development and prevent dental caries. However, if the human body uptakes excessive fluoride for a long time, it will lead to bone, teeth, and other tissue damage, such as skeletal and dental fluorosis [4,5], or even cause bone deformation and osteoporosis disease. Over the past decade, several studies have been focused on the effects

* Corresponding authors.

of environmental toxins on the human endocrine system, including the impact of fluoride on the thyroid gland [6]. A high F^- intake may cause serious toxic effects in consumers such as anemia in pregnancy, low birth weight babies, neurological problems and lowered IQ, chronic cognitive impairment and dementia, disturbed thyroid hormone metabolism, and infertility problems [7]. The World Health Organization (WHO) considers the optimum range of fluoride concentration in drinking water is 0.5–1.5 mg/L [8]. However, China suffers from endemic fluorosis in drinking water. Fluoride-bearing groundwater is widely distributed in China, there are still about 70 million people, who are still using excessive fluoride water, especially in northeast, north, and northwest China [9]. The production of industry, such as metal smelting, fluorine ore mining, chemical fertilizers, and pesticides, will produce high fluoride wastewater. There are still many residents suffering from endemic fluorosis of drinking water, because there is no satisfying method/equipment to effectively treat the high fluoride wastewater. Therefore, it is necessary to study the economical and efficient method for fluoride removal in water.

At present, there are many methods to remove fluoride ions from drinking water, including nanofiltration [10], sedimentation [11], electrocoagulation [12,13], electrodialysis [14], reverse osmosis [15], adsorption [16], and ion exchange [17]. Among these methods, adsorption is considered as one of the most promising methods because of its simple operation, low cost, and environmentally friendly property [18]. Commonly used adsorbents are bone charcoal, activated alumina, zeolite, and so on. In recent years, hydroxyapatite and zirconia with high fluoride adsorption capacity were also reported. By using these adsorbents, the concentration of less than 10 mg/L of fluoride-bearing water can be reduced to 1.0 mg/L, so as to meet the drinking water standard. Among many adsorbents, MgO is nontoxic due to its strong affinity, high adsorption capacity, and limited solubility in water [19]. In addition, the element of Mg accounts for about 2.3% on earth, which makes it cost-effective [20]. Therefore, it can be studied and widely used as an adsorbent. Compared with ordinary block materials, nanomaterials have larger surface areas and expose more surface atoms, thus showing stronger adsorption characteristics. Zhao et al. [21] prepared a new type of magnetic nano adsorbent, which used hydrated alumina containing Fe_3O_4 nanoparticles (Fe_3O_4@$Al(OH)_3$ nps) as the adsorbent. The adsorption capacity calculated by the Langmuir equation was 88.48 mg/g at pH = 6.5. Chai et al. [22] developed a new type of adsorbent by using sulfur-doped Fe_3O_4/Al_2O_3 nanoparticles as adsorbent. Langmuir model was used to calculate that the fluoride adsorption capacity was 70.4 mg/g at pH = 7.0. Mesbah et al. [23] synthesized a $LaFeO_3$ nanoparticle adsorbent. The results showed that under optimal conditions of fluoride concentration of 20 mg/L, the maximum percentage removal of 94.75% was obtained. Igwegbe et al. [24] investigated the efficacy of nickel oxide nanoparticles (NiO NPs). The results also showed that fluoride adsorption by NiO NPs was more compatible with the Freundlich isotherm, and the process followed the pseudo-second-order kinetic. Rahdar et al. [25] prepared Iron oxide nanoparticle and showed that the optimal adsorption conditions were as follows: pH 6, Fe_3O_4-NPs 0.02 g/L, initial fluoride 25 mg/L, contact time 45 min, and temperature 25°C. Ahmadi et al. [26] synthesized P/γ-Fe_2O_3 nanoparticles. The results presented an effective method for the removal of fluoride from water.

In this paper, a novel flower-shaped $Na_2Mg(CO_3)_2$ nanocomposite was synthesized through a one-step hydrothermal method. The adsorption isotherm and adsorption kinetics of the fluoride adsorption were studied. The $Na_2Mg(CO_3)_2$ materials were characterized by scanning electron microscopy (SEM), X-ray diffraction (XRD), Fourier transform infrared (FT-IR), and energy dispersive spectrum (EDS). Besides, the effect of pH and co-existing anions on the removal of fluoride adsorption were also studied. Based on the experimental results, the removal mechanism of fluoride ions was also discussed.

2. Experimental

2.1. Reagents and instruments

The reagents used in the experiment mainly include magnesium sulfate heptahydrate, sodium carbonate, sodium fluoride, acetic acid, sodium chloride, trisodium citrate, and sodium hydroxide; anhydrous ethanol, analytical purity, Xilong Scientific Co., Ltd., (China). Deionized water is prepared by FST-TOP-A24 super pure water equipment by Shanghai Fushite Instrument Equipment Co., Ltd., (China).

The instruments used in the experiment mainly include TG16K-Ⅱ table high speed centrifuge, Shanghai Zhaodi Biotechnology Co., Ltd., (China). RCT basic magnetic stirrer, EKA Instrument Equipment Co., Ltd., (China). DHG-9023A air drying box, Shanghai Yiheng Scientific Instrument Co., Ltd., (China). PHS-3C conductivity meter, Shanghai Instrument Co., Ltd., (China). CSB-F-2 fluoride ion selective electrode, Chengdu RuiXin Instrument Co., Ltd., (China). 9XL-1008 muffle furnace, Shanghai Jinghong Experimental Equipment Co., Ltd., (China). PHB-3 digital pH meter, Shanghai SanXin Instrument Factory (China). The XRD patterns of the adsorbents were performed on a D/MaxIIIA X-ray diffractometer (Rigaku Co., Japan), by using Cu Kα ($\lambda K\alpha 1$ = 1.5418 Å) as the radiation source in the range of 5°–80°. SEM image of the adsorbent was obtained with a FEI Quanta 200 FEG field emission scanning electron microscopy. The EDS and elemental mapping were performed on a Zeiss Auriga microscopy (Germany) equipped with an Oxford Inca X-Max 50 detector. The FT-IR spectra of the adsorbents before and after adsorption were recorded with a NEXUS-870 FT-IR spectrometer (Thermo Fisher Scientific in USA) in the range of 4,000–400 cm^{-1}.

2.2. Preparation of adsorbent

The flower-like $Na_2Mg(CO_3)_2$ nanoparticles adsorbent was synthesized through a one-step hydrothermal method [27]. In the process of synthesis, $MgSO_4{\cdot}7H_2O$ and Na_2CO_3 were prepared with molar ratio of 1:5. The weighted solid were dispersed in a beaker with 100 mL of ultra-pure water and vigorously stirred with a magnetic stirrer for 30 min. Then, the dispersed solution was placed into 100 mL of PTFE lined reactor. For the hydrothermal reaction, the temperatures of 80°C and heating durations of 12 h were employed. After cooling to room temperature, the obtained product was collected by filtration, washed with absolute ethanol and

ultra-pure water for several times. After that, the product was dried at 60°C for 12 h. The as-dried product was finally calcined in a muffle furnace at 300°C for 4 h to obtain the optimal material.

2.3. Batch adsorption experiments

To obtain a concentration of 1,000 mg/L fluoride standard solution, we dissolved 2.21 g of NaF in a beaker with 100 mL of ultra-pure water, and transferred it into a 1 L volumetric flask. All the solutions for fluoride removal experiments and analysis were prepared by diluting the stock solution to given concentration with ultra-pure water. The calibration curve was calculated by the potential of the standard sodium fluoride solutions (1–50 mg/L) at pH = 7. The pH value was adjusted by using 0.1 mol/L HCl and NaOH solution.

The adsorption capacity and removal rate of fluorine ions were calculated by Eqs. (1) and (2), respectively.

$$q_e = \frac{(C_0 - C_e)V}{m} \tag{1}$$

$$\eta = \frac{\left(C_0 - C_e\right)}{C_0} \times 100\% \tag{2}$$

where C_0 and C_e represent the initial and equilibrium fluoride concentration (mg/L), respectively, V (mL) is the volume of solution, and m (g) is the amount of the adsorbent.

The kinetics studies were carried out by a 200 mL fluoride standard solution with a concentration of 5 mg/L at 35°C. The adsorbent dose was set at 1 g/L with the pH = 7. After moving the solution into 250 mL of conical flask, 0.2 g adsorbent was added in it. The residual concentration of fluoride in the solution was measured by the fluoride ion-selective electrode and the adsorption capacity q_t (mg/g) was calculated as the function of time t (min). The adsorption isotherm studies were conducted by 30 mL fluoride standard solution with various initial concentrations. After moving them into 50 mL centrifuge tubes, 0.03 g adsorbent was added into each centrifuge tube and put it into a constant temperature shaking table at 150 rpm for 12 h. Then the initial concentration C_0 (mg/L) and equilibrium concentration C_e (mg/L) of fluoride in the solution were measured by the fluoride ion-selective electrode. After that, the equilibrium adsorption capacity q_e (mg/g) was calculated. The effect of pH and co-existing anions on the fluoride adsorption was studied at 35°C, 150 rpm, and 12 h. The effect of pH on the fluoride adsorption was conducted by using the initial fluoride concentration of 5 mg/L, with 1 g/L of adsorbent and a total fluoride solution volume of 20 mL. Five various anions were considered on the fluoride adsorption, such as sulfate, nitrate, chloride, bicarbonate, and phosphate, with the adsorbent dose of 1 g/L and an initial fluoride concentration of 5 mg/L at pH = 7. The co-existing anions were set at several concentration levels of 20, 30, 40, and 50 mg/L, respectively. By using the same method, the adsorption capacity of adsorbent was obtained. For evaluating the regeneration of adsorbents, fluoride-adsorbed $Na_2Mg(CO_3)_2$ were soaked into sodium hydroxide solution (3 wt.%) to be desorbed for fluoride adsorption again. Six consecutive adsorption–desorption cycles were performed to explore the regeneration of the $Na_2Mg(CO_3)_2$ adsorbent.

3. Results and discussion

3.1. Sample characterization

SEM images can show the detailed surface morphologies for the tested samples, which reveal the particle size and highly porous structure [28]. The morphology of the $Na_2Mg(CO_3)_2$ nanoparticles is obtained by SEM, as shown in Fig. 1. Both Figs. 1a and b are from samples before adsorption. The adsorbent presents a flower-like morphology. The diameter of the adsorbent is around 3.5 μm, as seen in Fig. 1b. The surface of adsorbent is smooth and the tiny gap from each other with closely arranged. Many of the layered sheet structures stack together, showing that the adsorbent has a larger specific surface area. Figs. 1c and d are the images for the samples after adsorption. The adsorbent still presents a flower-like morphology compared with the one before adsorption, but the surface is no longer smooth due to the loose layered sheet structure. Actually, it was covered with a thick powdery substance. The gap between the adsorbents became larger, and the arrangement is no longer compact. The crystalline structure of the samples are identified by XRD pattern [29,30]. The crystal structures of the final products were measured by powder X-ray diffractometric analysis shown in Fig. 2. It can be seen that all diffraction peaks of the resulting products can be indexed to the sodium magnesium carbonate ($Na_2Mg(CO_3)_2$, JCPDS card no. 00–024–1227). The diffraction peaks at 2θ = 23.42°, 32.76°, 34.44°, 36.35°, 40.02°, 42.59°, 43.67°, 47.90°, 49.69°, 50.90°, 57.17°, 60.41°, 63.38°, 64.15°, 65.37°, 67.85°, and 68.62° can be, respectively, indexed to (012), (006), (015), (110), (113), (021), (202), (024), (116), (205), (211), (1010), (119), (125), (300), (303), and (0012) planes of sodium magnesium carbonate in rhombohedral structure. The EDS spectrum of $Na_2Mg(CO_3)_2$ nanoparticles is shown in Fig. 3 and the elemental composition after fluoride adsorption of $Na_2Mg(CO_3)_2$ nanoparticles are listed in Table 1. It verifies the presence of carbon, oxygen, magnesium, sodium, and fluoride elements when the adsorbent has finished the process of fluoride adsorption.

3.2. Adsorption isotherm

To study the adsorption performance of the adsorbent, the adsorption equilibrium of fluoride removal is usually fitted by Langmuir and Freundlich adsorption isotherm model, and the linear Eqs. (3) and (4), respectively. The corresponding parameters of two models are listed in Table 2. There is a comparison of adsorption capacity with various adsorbents in Table 3. To the best of our knowledge, the as-synthesized $Na_2Mg(CO_3)_2$ nanoparticles have a relatively higher adsorption capacity than that of others.

$$\frac{C_e}{q_e} = \frac{C_e}{q_m} + \frac{1}{K_L q_m} \tag{3}$$

$$\ln q_e = \frac{1}{n}\ln C_e + \ln K_F \tag{4}$$

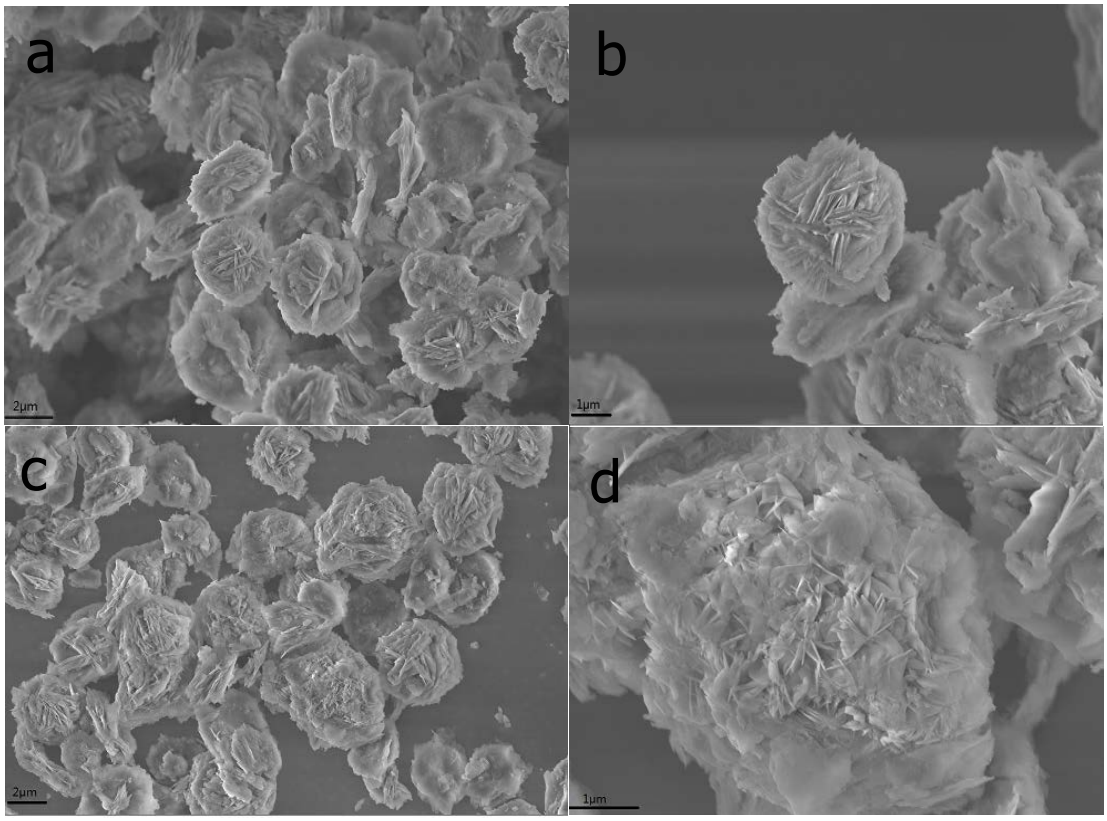

Fig. 1. SEM images of $Na_2Mg(CO_3)_2$ nanoparticles, (a and b) before adsorption, (c and d) after adsorption.

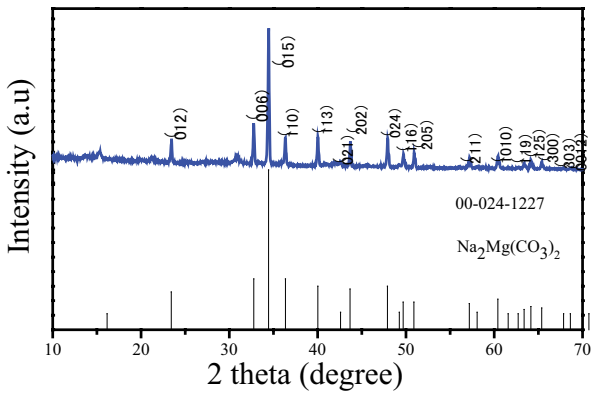

Fig. 2. XRD pattern of $Na_2Mg(CO_3)_2$ nanoparticles adsorbent.

where C_e (mg/L) is the fluorine concentration after equilibrium adsorption; q_e (mg/g) is the amount of defluoridation on per weight of the adsorbent after equilibrium; q_m (mg/g) is the maximum adsorption capacity calculated according to Langmuir equation; K_L (L/mg) is the Langmuir adsorption constant; K_F (mg/g), and n are Freundlich adsorption constant.

Both Freundlich and Langmuir models are applied to fit the experimental adsorption results as shown in Fig. 4. The calculated results of two models are shown in Table 2. The Freundlich isotherm model gives a better fit to the experimental data than the Langmuir isotherm model with the correlation coefficient value(R) of 0.995. When the initial concentration of fluoride is 200 mg/L, the maximum adsorption capacity calculated by Langmuir isotherm model is up to 113.64 mg/g at pH = 7 and 35°C. According to the above data, the $Na_2Mg(CO_3)_2$ nanoparticles show a good effect on fluoride adsorption.

3.3. Adsorption kinetics

Adsorption kinetics studies the adsorption rate of adsorbent, and the experimental data of adsorption kinetics are simulated with pseudo-first-order kinetics and pseudo-second-order kinetics models, respectively. The equations of pseudo-first-order kinetics and pseudo-second-order kinetics are as follows.

$$\log(q_e - q_t) = \log q_e - \frac{k_1 t}{2.303} \tag{5}$$

$$\frac{t}{q_e} = \frac{1}{k_2 q_e^2} + \frac{t}{q_e} \tag{6}$$

where q_e and q_t are the amount of fluoride adsorbed (mg/g) at equilibrium and at any time, respectively; t (min) is the adsorbed time. The k_1 (1/min) is the rate constant for pseudo-first-order reaction. The k_2 (g/(mg min)) is the rate constant for pseudo-second-order reaction.

The corresponding parameters of two models are calculated from the plots of $\ln(q_e - q_t)$ vs. t and (t/q_t) vs. t,

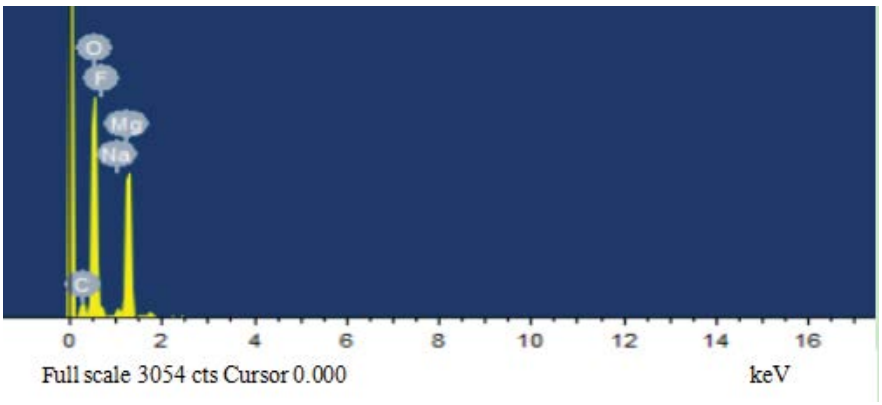

Fig. 3. EDS pattern of $Na_2Mg(CO_3)_2$ nanoparticles after adsorption.

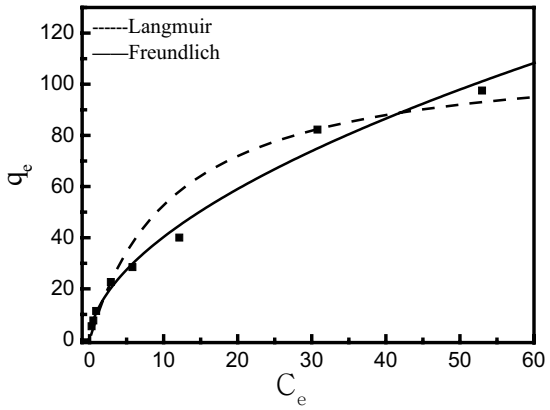

Fig. 4. Isotherm of fluoride adsorption by $Na_2Mg(CO_3)_2$.

respectively. The linear correlation coefficient value (R) and the kinetic parameters are listed in Table 4. According to Fig. 5a, the adsorption capacity increased rapidly at the beginning of 0–10 min. At the stage of 10–100 min, the adsorption rate gradually slows down. In the following 100–360 min, the adsorption capacity tends to be stable and reaches the maximum value. So the adsorption equilibrium time is 100 min. According to the Table 4, it showed the pseudo-second-order kinetics model gives a better fit to the experimental data than the pseudo-first-order model with the linear correlation coefficient value (R) of 0.999. The calculated value of q_e = 42.553, which is almost similar to the experimental value of q_e = 41.48 when the initial fluoride concentration is 5 mg/L.

3.4. Effect of pH on fluoride adsorption

In most solid–liquid adsorption, the pH of the solution has a great influence on the adsorption of the adsorbent. In this paper, fluoride removal effect of $Na_2Mg(CO_3)_2$ nanoparticles at different pH (3–12) was tested. It can be clearly seen from Fig. 6 that the pH value has little effect on $Na_2Mg(CO_3)_2$ nanoparticles on the fluoride adsorption within the range of wide pH (3–10). The fluoride removal rate reaches up to 92.26% at pH = 7 for initial fluoride concentration of 5 mg/L, along with the adsorbent dose of 1 g/L. Besides, the rest of

Table 1
Elemental composition of the synthesized $MgO/MgCO_3$ nanoparticles after adsorption

Elements	Weight %	Atomic %
C K	0.51	13.55
O K	3.10	61.17
F K	0.48	7.97
Na K	0.06	0.80
Mg K	1.27	16.51
Totals	5.42	100

fluoride concentration is about 0.39 mg/L. Under the condition of strong alkalinity (pH ≥ 11), the removal rate of adsorbent decreased obviously, which may be caused by more hydroxyl competing with fluoride for the active sites on the adsorbent and electrostatic repulsion on the surface of the adsorbent, resulting in the decrease of removal rate [41].

3.5. Effect of co-existing anions

In actual groundwater, many anions coexist with fluoride, so it is of great significance to study the interference of co-existing ions on fluoride adsorption. As shown in Fig. 7, compared with the blank sample, the presence of phosphate, nitrate, sulfate, carbonate, and chloride showed little effect on the removal rate of fluoride at lower concentrations of 20 and 30 mg/L. while the presence of phosphate, sulfate, and carbonate affected the removal efficiency at relatively high concentrations of 40 and 50 mg/L. Compared to the lower concentration, the removal rate of interference of these three ions were relatively obvious. The decrease of removal rate of $Na_2Mg(CO_3)_2$ adsorbent may be caused by the competition with the active sites on the surface of adsorbent between phosphate, sulfate, carbonate, and fluoride. The removal rate of these three ions was $SO_4^{2-} > HCO_3^- > PO_4^{3-}$.

FT-IR can provide the molecular and structural information about organic and inorganic materials [42]. Fig. 8 shows the FT-IR of $Na_2Mg(CO_3)_2$ nanoparticles fluoride adsorption. The reported Mg–F stretching vibration of MgF_2

Table 2
Parameters of Langmuir and Freundlich adsorption isotherm model

Isotherm model	Langmuir $\frac{C_e}{q_e}=\frac{C_e}{q_m}+\frac{1}{K_L\times q_m}$			Freundlich $\ln q_e=\frac{1}{n}\ln C_e+\ln K_F$		
Parameters	(L/mg)	(mg/g)	R^2	n	K_F	R^2
Value	0.087	113.64	0.907	1.81	11.30	0.995

Table 3
Comparison of adsorption capacity with different adsorbents and the corresponding parameters

Adsorbents	pH	Temperature (°C)	Adsorption capacity(mg/g)	Reference
Fe–Ti oxide	7	25	31.24	[31]
Mg–Al bimetallic oxides	6	298 K	89.3	[32]
CeO_2–ZrO_2 nanocages	4	25	175	[33]
CTAB assisted mixed iron oxide	5	25	40.4	[34]
Zirconium-modified-Na-attapulgite	4.13	323K	24.55	[35]
Trititanate nanotubes (TNT)	2	353 K	58	[36]
Montmorillonite and bentonite nanoparticles	3	–	5.5	[37]
Nanochitosan	3	–	9	[38]
Zirconium SPADN	–	–	1.56	[39]
Silica nanoparticles	3	–	8.4	[40]
Flower-shaped $Na_2Mg(CO_3)_2$ nanoparticle	7	35	113.64	Present work

Table 4
Parameters of pseudo-first and second-order kinetics model

Kinetics model	Pseudo-first-order		Pseudo-second-order		
k_1 (1/min)	q_e (mg/g)	R^2	k_2 (g/mg min)	q_e (mg/g)	R^2
0.018	16.955	0.870	3.87×10^{-3}	42.553	0.999

has a strong shoulder peak at 400–500 cm^{-1}. So, the new observed FT-IR peak at 409 cm^{-1} in Fig. 8b may be attributed to the Mg–F stretching vibration [43]. The peak at 409 cm^{-1} is formed, which is very closer to the range of Mg–F stretching vibration, though it is very weak [44]. As shown in Fig. 8a, the absorption peaks at 714 and 596 cm^{-1} can be attributed to the vibration of Mg–O [45]. Furthermore, the peaks at 1,120 (ν_1 mode), 1,480 and 1,420 (ν_3 mode) confirm the presence of a CO_3^{2-} cm^{-1} group. The FT-IR peak at 3,450 cm^{-1} can be attributed to the physically adsorbed water [46]. After fluoride adsorption, the peak at 3,690 cm^{-1} is ascribed to the lattice vibration of $Mg(OH)_2$ [47,48]. Moreover, after fluoride removal, the peaks at 1,120 (ν_1 mode), 1,480 and 1,420 (ν_3 mode), turn relatively weak indicating carbonate ions partly lost, which verified the important roles of CO_3^{2-} in the adsorption of fluoride. Therefore, the fluoride removal may be a surface ion-exchange process based on CO_3^{2-} and surface hydroxyl ions exchanged with F^-.

3.6. Regeneration and reuse of the adsorbent

The regeneration results after six adsorption–desorption cycles with the initial fluoride concentration of 5 mg/L, pH = 7, and the adsorbent dose of 1 g/L, are shown in Fig. 9. The removal rates of adsorbents are 92.16%, 91.31%, 89.62%, 88.05%, 85.49%, and 83.67%, respectively. It shows that the efficacy of the adsorbents still maintains high as being reused repeatedly, indicating that the spent adsorbent is suitable for regeneration.

4. Conclusion

The flower-like $Na_2Mg(CO_3)_2$ nanocomposite adsorbent is synthesized through a simple hydrothermal method, which shows a good adsorption performance for removing fluoride ions. When pH = 7 and the temperature is 35°C, the adsorption isotherm fits the Freundlich model. When the

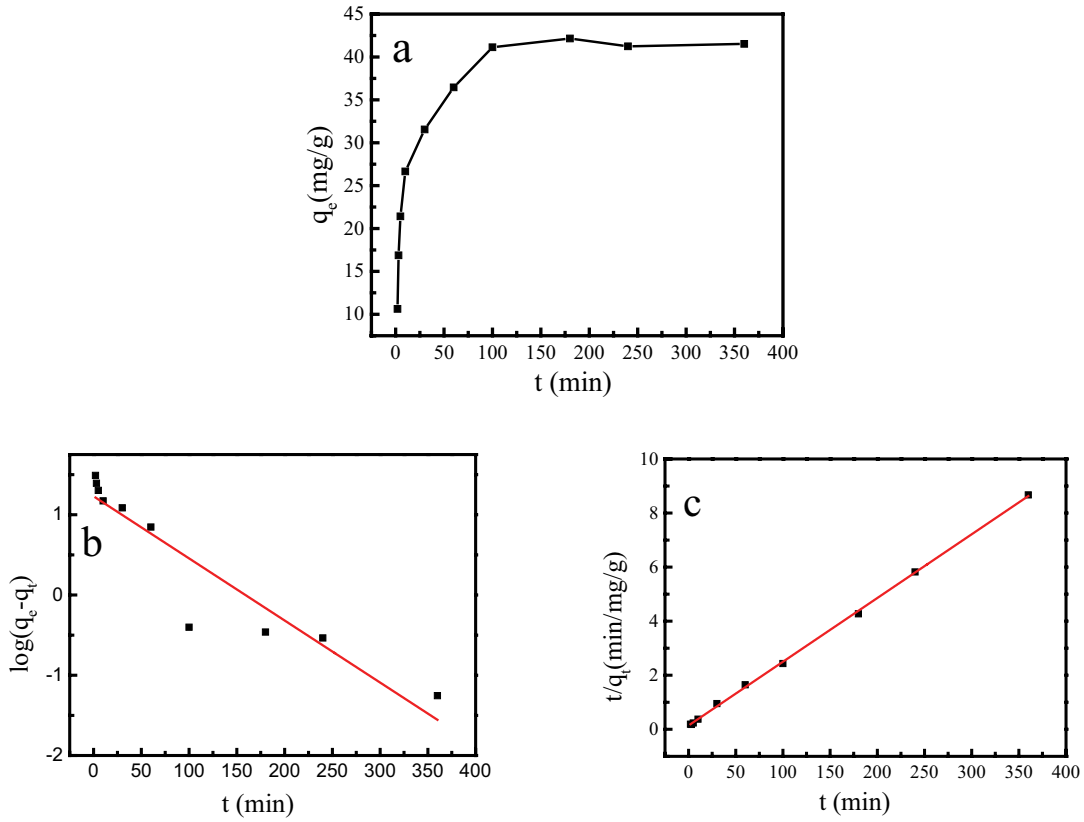

Fig. 5. (a) Plot for the experimental data of the kinetics of fluoride removal; (b) and (c) plots for the pseudo-first and pseudo-second-order kinetic fitting of fluoride adsorption, respectively.

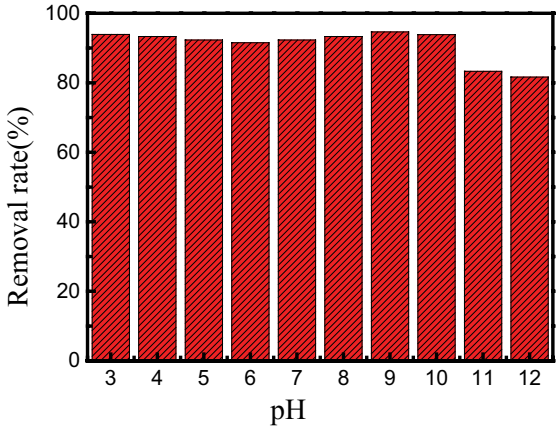

Fig. 6. Effect of pH on fluoride adsorption.

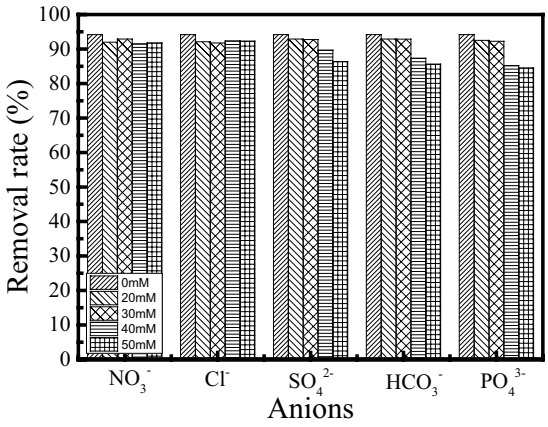

Fig. 7. Effect of co-existing anions on fluoride adsorption.

initial concentration is 200 mg/L, the maximum adsorption capacity calculated by the Langmuir model could reach up to 113.64 mg/g. The adsorption kinetics is consistent with the pseudo-second-order model, and the adsorption equilibrium can be achieved within 100 min. In the range of wide pH values (3–10), it has little effect on $Na_2Mg(CO_3)_2$ fluoride adsorption. The fluoride removal rate is 92.26% at pH = 7 for the initial fluoride concentration of 5 mg/L, with the adsorbent dose of 1 g/L. Except for the PO_4^{3-}, SO_4^{2-}, and HCO^{3-}, other anions almost have not effected on the fluoride adsorption. The experimental results indicate that the adsorbent can be reused for more than six times. The presented findings are expected to provide a basis for the practical application of fluoride removal in drinking water.

Acknowledgments

This work was supported by the Project of National Key Research and Development Program (2019YFC0408503), the Natural Science Major Research Projects of Anhui

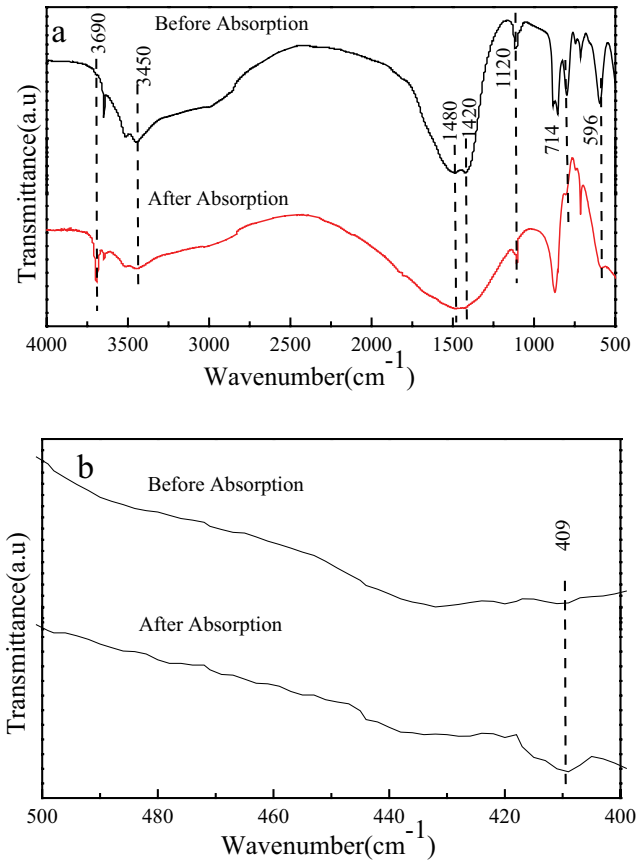

Fig. 8. (a and b) FT-IR spectra of $Na_2Mg(CO_3)_2$ before and after fluoride adsorption.

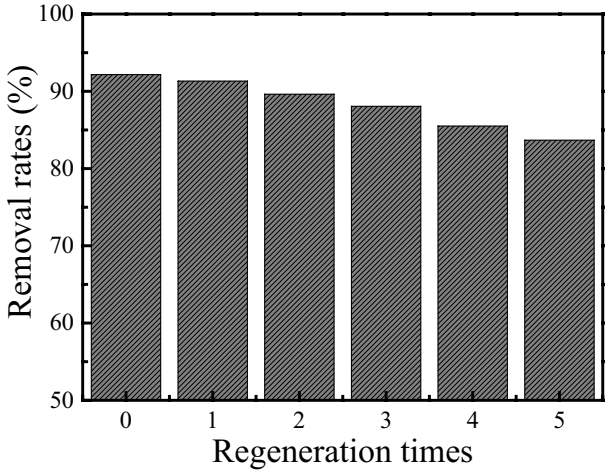

Fig. 9. Regeneration test of adsorbent.

Education Department (KJ2017ZD40), the National Natural Science Foundation of China (61873003, 21677001), the Science and Technology Major projects of Anhui Province (18030801106,16030801118), the Key Research and Development Plan of Anhui Province (201904a07020070), and the Scientific Research Start-up Foundation for Introduction of Talent, Anhui Jianzhu University (2016QD113).

References

[1] E.J. Reardon, A limestone reactor for fluoride removal from wastewaters, Environ. Sci. Technol., 34 (2000) 3247–3253.
[2] F. Shen, X.M. Chen, P. Gao, Electrochemical removal of fluoride ions from industrial wastewater, Chem. Eng. Sci., 58 (2003) 987–993.
[3] M. Yousefi, M. Ghoochani, A.H. Mahvi, Health risk assessment to fluoride in drinking water of rural residents living in the Poldasht city, Northwest of Iran, Ecotoxicol. Environ. Saf., 148 (2018) 426–430.
[4] A. Rahmani, K. Rahmani, S. Dobaradaran, A.H. Mahvi, R. Mohamadjani, H. Rahmani, Child dental caries in relation to fluoride and some inorganic constituents in drinking water in Arsanjan, Iran, Fluoride, 43 (2010) 179–186.
[5] A.A. Mohammadi, M. Yousefi, M. Yaseri, M. Jalilzadeh, A.H. Mahvi, Skeletal fluorosis in relation to drinking water in rural areas of West Azerbaijan, Iran, Sci. Rep., 7 (2017) 1–7, doi: 10.1038/s41598-017-17328-8.
[6] Z. Kheradpisheh, M. Mirzaei, A.H. Mahvi, M. Mokhtari, R. Azizi, H. Fallahzadeh, M.H. Ehrampoush, Impact of drinking water fluoride on human thyroid hormones: a case-control study, Sci. Rep., 8 (2018) 2674–2680.
[7] M. Yousefi, A.A. Mohammadi, M. Yaseri, A.H. Mahvi, Epidemiology of drinking water fluoride and its contribution to fertility, infertility, and abortion: an ecological study in west Azerbaijan province, Poldasht county, Iran, Fluoride, 50 (2017) 343–353.
[8] H.G. Gorchev, G. Ozolins, WHO Guidelines for Drinking-Water Quality, World Health Organization, Geneva, 1984.
[9] L.D. Kong, J.X. He, A.Y. Wang, The progress of the research on the treatment of the fluorine-containing sewage, Sci. Tech. Inform. Dev. Econ., 16 (2006) 46–48.
[10] S.V. Jadhav, K.V. Marathe, V.K. Rathod, A pilot scale concurrent removal of fluoride, arsenic, sulfate and nitrate by using nanofiltration: competing ion interaction and modelling approach, J. Water Process Eng., 13 (2016) 153–167.
[11] H.B. Cong, F. Sun, W.J. Chen, Study on the method and mechanism of pre-pressure coagulation and sedimentation for microcystis removal from drinking-water sources, Environ. Technol., 39 (2018) 433–449.
[12] A.R. Donovan, C.D. Adams, Y.F. Ma, Fate of nanoparticles during alum and ferric coagulation monitored using single particle ICP-MS, Chemosphere, 195 (2017) 531–541.
[13] E. Bazrafshan, K.A. Ownagh, A.H. Mahvi, Application of electrocoagulation process using iron and aluminum electrodes for fluoride removal from aqueous environment, J. Chem., 9 (2012) 2297–2308.
[14] F.D. Belkada, O. Kitous, N. Drouiche, Electrodialysis for fluoride and nitrate removal from synthesized photovoltaic industry wastewater, Sep. Purif. Technol., 204 (2018) 108–115.
[15] I. Parlar, M. Hacıfazlıoğlu, N. Kabay, Performance comparison of reverse osmosis (RO) with integrated nanofiltration (NF) and reverse osmosis process for desalination of MBR effluent, J. Water Process Eng., 29 (2019) 1–7, doi: 10.1016/j.jwpe.2018.06.002.
[16] D.J. Kang, X.L. Yu, M.F. Ge. Morphology-dependent properties and adsorption performance of CeO_2 for fluoride removal, Chem. Eng. J., 330 (2017) 36–43.
[17] Y.X. Zhang, Y. Jia, Fluoride adsorption on manganese carbonate: ion-exchange based on the surface carbonate-like groups and hydroxyl groups, J. Colloid Interface Sci., 510 (2017) 407–417.
[18] X. Fan, D.J. Parker, M.D. Smith, Adsorption kinetics of fluoride on low cost materials, Water Res., 37 (2003) 4929–4937.
[19] A. Bhatnagar, E. Kumar, M. Sillanpää, Fluoride removal from water by adsorption - a review, Chem. Eng. J., 171 (2011) 811–840.
[20] S.S. Fu, P.J. Li, F. Qian, Soil quality degradation in a magnesite mining area, Pedosphere, 21 (2011) 98–106.
[21] X.L. Zhao, J.M. Wang, F.C. Wu, Removal of fluoride from aqueous media by Fe_3O_4@$Al(OH)_3$ magnetic nanoparticles, J. Hazard. Mater., 173 (2010) 102–109.
[22] L.Y. Chai, Y.Y. Wang, N. Zhao, Sulfate-doped Fe_3O_4/Al_2O_3 nanoparticles as a novel adsorbent for fluoride removal from drinking water, Water Res., 47 (2013) 4040–4049.

[23] M. Mesbah, S. Hamedshahraki, S. Ahmadi, M. Sharifi, C.A. Igwegbe, Hydrothermal synthesis of $LaFeO_3$ nanoparticles adsorbent: characterization and application of error functions for adsorption of fluoride, MethodsX, 7 (2020) 1–15, doi: 10.1016/j.mex.2020.100786.
[24] C.A. Igwegbe, S. Rahdar, A. Rahdar, A.H. Mahvi, S. Ahmadi, A.M. Banach, Removal of fluoride from aqueous solution by nickel oxide nanoparticles: equilibrium and kinetic studies, Fluoride, 52 (2019) 569–579.
[25] A. Rahdar, S. Ahmadi, J. Fu, S. Rahdar, Iron oxide nanoparticle preparation and its use for the removal of fluoride from aqueous solution: application of isotherm, kinetic and thermodynamics, Desal. Water Treat., 137 (2019) 174–182.
[26] S. Ahmadi, S. Rahdar, C.A. Igwegbe, A. Rahdar, N. Shafighi, F. Sadeghfar, Data on the removal of fluoride from aqueous solutions using synthesized P/γ-Fe_2O_3 nanoparticles: a novel adsorbent, MethodsX, 6 (2019) 98–106.
[27] K.S. Zhang, S.B. Wu, X.L. Wang, J.Y. He, L.T. Kong, J.H. Liu, Wide pH range for fluoride removal from water by MHS-MgO/$MgCO_3$ adsorbent: kinetic, thermodynamic and mechanism studies, J. Colloid Interface Sci., 446 (2015) 194–202.
[28] N. Minju, K.V. Swaroop, K. Haribabu, Removal of fluoride from aqueous media by magnesium oxide-coated nanoparticles, Desal. Water Treat., 53 (2015) 2905–2914.
[29] A. Naghizadeh, M. Ghafouri, Synthesis and performance evaluation of chitosan prepared from Persian gulf shrimp shell in removal of reactive blue 29 dye from aqueous solution (isotherm, thermodynamic and kinetic study), Iran. J. Chem. Chem. Eng., 36 (2017) 25–36.
[30] A. Naghizadeh, S. Nasseri, A.H. Mahvi, R. Nabizadeh, R.R. Kalantary, A. Rashidi, Continuous adsorption of natural organic matters in a column packed with carbon nanotubes, J. Environ. Health Sci. Eng., 14 (2013) 25–31.
[31] L. Chen, B.Y. He, S. He, Fe–Ti oxide nano-adsorbent synthesized by co-precipitation for fluoride removal from drinking water and its adsorption mechanism, Powder Technol., 227 (2012) 3–8.
[32] S. Moriyama, K. Sasaki, T. Hirajima, Effect of calcination temperature on Mg-Al bimetallic oxides as sorbents for the removal of F^- in aqueous solutions, Chemosphere, 95 (2014) 597–603.
[33] J. Wang, W.H. Xu, L. Chen, Excellent fluoride removal performance by CeO_2-ZrO_2 nanocages in water environment, Chem. Eng. J., 2319 (2013) 198–205.
[34] M. Mohapatra, K. Rout, P. Singh, Fluoride adsorption studies on mixed-phase nano iron oxides prepared by surfactant mediation-precipitation technique, J. Hazard. Mater., 186 (2011) 1751–1757.
[35] G.K. Zhang, Z.L. He, W. Xu, A low-cost and high efficient zirconium modified Na attapulgite adsorbent for fluoride removal from aqueous solutions, Chem. Eng. J., 183 (2012) 315–324.
[36] P. Chinnakoti, R.K. Vankayala, A.L.A. Chunduri, Trititanate nanotubes as highly efficient adsorbent for fluoride removal from water: adsorption performance and uptake mechanism, J. Environ. Chem. Eng., 4 (2016) 4754–4768.
[37] A. Naghizadeh, K. Gholami, Bentonite and montmorillonite nanoparticles effectiveness in removal of fluoride from water solutions, J. Water Health, 15 (2017) 555–565.
[38] A. Naghizadeh, H. Shahabi, E. Derakhshani, F. Ghasemi, A.H. Mahvi, Synthesis of nanochitosan for the removal of fluoride from aqueous solutions: a study of isotherms, kinetics, and thermodynamics, Fluoride, 50 (2017) 256–268.
[39] A. Karimi, M. Radfard, M. Abbasi, A. Naghizadeh, H. Biglari, V. Alvani, M. Mahdavi, Fluoride concentration data in ground water resources of Gonabad, Iran, Data Brief, 21 (2018) 105–110.
[40] F. Masoudi, A. Naghizadeh, Silica nanoparticles for the removal of fluoride from aqueous solution: equilibrium, isotherms, kinetics and thermodynamics, Desal. Water Treat., 137 (2019) 125–133.
[41] R.R. Devi, I.M. Umlong, P.K. Raul, Defluoridation of water using nano-magnesium oxide, J. Exp. Nanosci., 9 (2014) 512–524.
[42] M. Kamranifar, A. Naghizadeh, Montmorillonite nanoparticles in removal of textile dyes from aqueous solutions: study of kinetics and thermodynamics, Iran. J. Chem. Chem. Eng., 36 (2017) 127–137.
[43] H.A. Prescott, Z.J. Li, E. Kemnitz, Application of calcined Mg–Al hydrotalcites for Michael additions: an investigation of catalytic activity and acid–base properties, J. Catal., 234 (2005) 119–130.
[44] H.X. Niu, Q. Yang, K.B. Tang, Large-scale synthesis of single-crystalline MgO with bone-like nanostructures, J. Nanopart. Res., 8 (2006) 881–888.
[45] Y.D. Zou, X.X. Wang, F. Wu, Controllable synthesis of Ca-Mg-Al layered double hydroxides and calcined layered double oxides for the efficient removal of U(VI) from wastewater solutions, ACS Sustainable Chem. Eng., 5 (2017) 1173–1185.
[46] Z.P. Zhang, Y.J. Zheng, Y.W. Ni, Temperature and pH-dependent morphology and FT-IR analysis of magnesium carbonate hydrates, J. Phys. Chem. B, 110 (2006) 12969–12973.
[47] Y.M. Liu, X.R. Li, R.L. Jia, Effects of biological soil crusts on soil nematode communities following dune stabilization in the Tengger Desert, Northern China, Appl. Soil Ecol., 49 (2011) 118–124.
[48] A.N. Christensen, P. Norby, J.C. Hanson, Chemical reactions in the system MgO–$MgCl_2$–H_2O followed by time-resolved synchrotron X-ray powder diffraction, J. Solid State Chem., 114 (1995) 556–559.